



## Stability of delta distributary networks and their bifurcations

D. A. Edmonds<sup>1</sup> and R. L. Slingerland<sup>1</sup>

Received 12 March 2008; revised 18 June 2008; accepted 23 June 2008; published 18 September 2008.

[1] Delta distributary networks are created by bifurcating channels that commonly split their discharges unequally. The origin and stability of these asymmetrical fine-grained cohesive bifurcations are investigated here using Delft3D, a morphodynamic flow and sediment transport model. Results are compared to bifurcations on the Mossy delta, Saskatchewan, Canada, that have remained stable for decades. Over a range of channel aspect ratios, friction factors, and Shields numbers, we find three equilibrium functions relating the discharge ratio of the bifurcate arms at equilibrium to the Shields number. One function defines symmetrical configurations (equal partitioning of discharge), while the other two define asymmetrical configurations (unequal partitioning of discharge). Discharge asymmetries and morphologies of Mossy delta bifurcations are consistent with these predictions. Among the equilibrium bifurcations, only the asymmetrical type is stable to perturbations, such as a partial closing of one throat. This possibly explains why asymmetrical bifurcations are more common in nature.

**Citation:** Edmonds, D. A., and R. L. Slingerland (2008), Stability of delta distributary networks and their bifurcations, *Water Resour. Res.*, 44, W09426, doi:10.1029/2008WR006992.

### 1. Introduction

[2] A survey of the world's river-dominated delta networks reveals that distributary channels rarely split their water discharges equally as they bifurcate into multiple channels. Rather, the discharges, and consequently the channel widths, depths, and sediment loads, are usually asymmetrical, seemingly representing a stable configuration (Figure 1). This regularity seems surprising given the complexity of distributary channel mechanics and suggests that morphodynamic feedbacks are at work acting to stabilize the delta channel network. Because it is the bifurcations that create the network, we focus on them here and ask these questions: (1) can asymmetrical bifurcations be in equilibrium such that the hydraulic properties of each bifurcate channel are adjusted to just transport the water and sediment given to it? (2) If so, are they stable, equilibrium configurations that return to their equilibrium configuration when perturbed? (3) Will perturbations such as climate change [e.g., *Ericson et al.*, 2006; *Lesack and Marsh*, 2007] and upstream impoundment of sediment by dams [*Syvitski et al.*, 2005], lead to increasing instabilities and degradation of these channel network and their bifurcations?

[3] These questions are important because the distributary networks that bifurcations create provide valuable maritime infrastructure and fertile floodplains to humans, and a nutrient-rich habitat for a diverse and biologically valuable ecosystem [*Olson and Dinerstein*, 1998]. Here we attempt to answer the first two questions using a numerical model and field data to elucidate how asymmetrical deltaic bifurcations function and under what conditions they are

stable. Bifurcations are stabilized by processes operating locally, such as division of sediment at the bifurcation point, and processes operating globally, such as delta-scale changes in water surface slope. We restrict our analysis of distributary network stability to those processes acting locally on the bifurcations.

### 2. Present Understanding of Fluvial-Channel Bifurcations

#### 2.1. General Characteristics of Bifurcations

[4] Among the occurrences of channel bifurcations we make the distinction between coarse-grained systems and fine-grained noncohesive and cohesive systems. The former seem to adjust their hydraulic geometry to maintain a Shields stress ( $\Theta$ ) at about 1.4 times the critical Shields stress [*Parker*, 1978], whereas the latter maintain a  $\Theta$  of about 1 for mixed load channels and about 10 for suspended load channels [*Dade and Friend*, 1998].  $\Theta$  is defined as

$$\Theta = \frac{\tau_o}{(\rho_s - \rho)gD_{50}} \quad (1)$$

where  $\tau_o$  is the fluid shear stress ( $\text{N/m}^2$ ),  $\rho_s$  is the sediment density ( $\text{kg/m}^3$ ),  $\rho$  is the water density ( $\text{kg/m}^3$ ),  $g$  is acceleration due to gravity ( $\text{m/s}^2$ ), and  $D_{50}$  is the median bed grain size (m).

[5] Even though coarse-grained (hereafter termed low  $\Theta$ ) and fine-grained (hereafter termed high  $\Theta$ ) bifurcations are thought to arise from different processes, ranging from flow splitting around bars to avulsion, they exhibit intriguingly organized and similar behaviors. On average, fluvial channel bifurcations are asymmetrical. *Edmonds and Slingerland* [2007] measured widths of the bifurcate channels on the world's distributary deltas and found that the width ratios cluster around 1.7:1 ( $n = 160$ ). A similar comprehensive study is missing for braided streams, but limited observa-

<sup>1</sup>Department of Geosciences, Pennsylvania State University, University Park, Pennsylvania, USA.

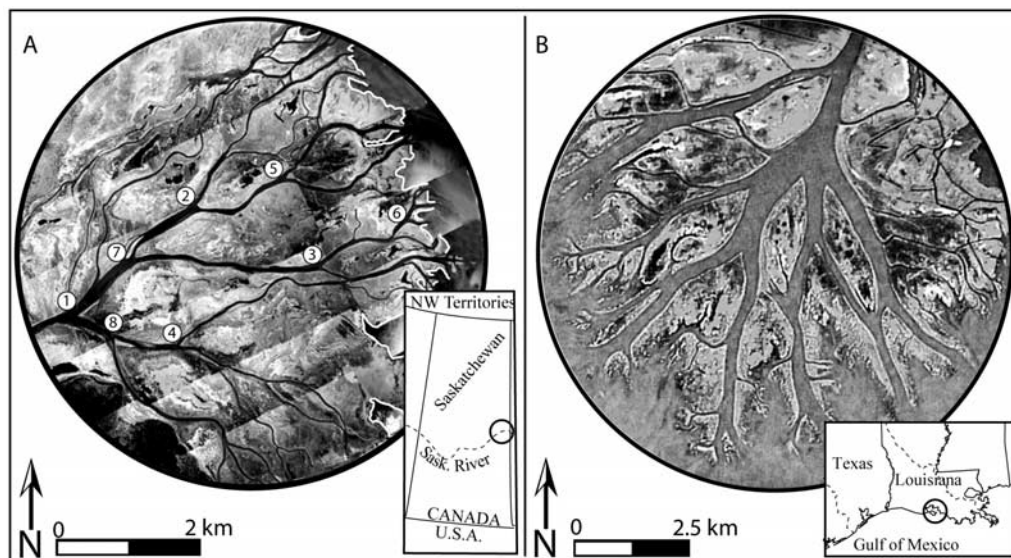


**Figure 1.** Two examples of distributary deltas with bifurcating channel networks. On average the fluvial channel bifurcations (wherein one channel splits into two) are asymmetrical; their bifurcate discharges are unequal. This is true for the bifurcations on the coastline and the more mature bifurcations farther up the delta. (A) Composite aerial photograph of Mossy Delta, Saskatchewan, Canada from 2003. Individual photos are from *Information Service Corporation of Saskatchewan* [2003]. The white line on the east side of the delta is the shoreline. The numbers mark the locations of the eight bifurcations in this study. (B) Image of Wax Lake Outlet delta, LA from 1998 USGS aerial photography. Inset maps shows delta locations marked by a circle.

tions suggest that bifurcate width ratios for braided streams cluster around 1.5:1 ( $n = 8$ ) [Zolezzi *et al.*, 2006]. For both cases, limited data indicate that channel widths are hydraulically adjusted to the discharge, and therefore the depths and discharges probably also are asymmetrical. The equilibrium configuration of asymmetrical bifurcations and their degree of stability are open and interesting questions that we will address in this study.

## 2.2. Low $\Theta$ Bifurcations

[6] By far the most studied bifurcation type has been within low  $\Theta$  channels, whether by field observation [Davoren and Mosley, 1986; Ashmore *et al.*, 1992; Ashworth *et al.*, 1992; Bridge, 1993; Ashworth, 1996; Richardson and Thorne, 2001; Zolezzi *et al.*, 2006; Frings and Kleinhans, 2008], flume studies [Federici and Paola, 2003; Zanichelli *et al.*, 2004; Bertoldi and Tubino, 2005; Islam *et al.*, 2006; Bertoldi and Tubino, 2007], or by numerical modeling [Repetto *et al.*, 2002; Bolla Pittaluga *et al.*, 2003; Dargahi, 2004; Zanichelli *et al.*, 2004; Hall, 2005; Wu and Yeh, 2005; Kleinhans *et al.*, 2008; Miori *et al.*, 2006].

[7] Present understanding of low  $\Theta$  bifurcation stability is summarized in Miori *et al.* [2006] and Bertoldi and Tubino [2007] who built on the pioneering approach of Bolla Pittaluga *et al.* [2003]. Bolla Pittaluga *et al.* [2003] approached the problem with a one-dimensional numerical model of steady, uniform flow through a bifurcation. They discovered that the bed ramp, defined as the topographic rise in elevation from the unbifurcated reach to the shallower of the two downstream channels, steered different amounts of bed load to each downstream channel enabling an asymmetrical stable, equilibrium solution. Their model predicts that as  $\Theta$  increases in the unbifurcated reach, the

stable, equilibrium bifurcate discharge ratio (larger channel/smaller channel) should decrease. Miori *et al.* [2006] improved on the Bolla Pittaluga model by allowing channel width to vary according to hydraulic geometry rules. They also produced asymmetrical stable, equilibrium bifurcations, and found that the final stable function depends on whether a bifurcation forms through incision of a new channel, or flow splitting around a midchannel bar. Other work has shown that stable solutions can be a function of an upstream meander bend [Kleinhans *et al.*, 2008] or the bifurcation angle magnitude [Mosselman *et al.*, 1995].

## 2.3. High $\Theta$ Bifurcations

[8] There has been much less research on high  $\Theta$  bifurcations. Only a few field studies exist [Axelsson, 1967; Andren, 1994; Sloff *et al.*, 2003; Edmonds and Slingerland, 2007], experimental studies are hampered by scaling considerations [Zanichelli *et al.*, 2004], and theoretical studies are limited to Wang *et al.* [1995] and Slingerland and Smith [1998].

[9] Development of an adequate stability theory for high  $\Theta$  bifurcations also lags behind the low  $\Theta$  case. It may be that the theory for low  $\Theta$  bifurcations also applies to high  $\Theta$  bifurcations; however, this idea is untested and hinges on what roles the suspended load and sediment cohesiveness play. Wang *et al.* [1995] considered a bifurcation where the two bifurcate channels flow into a lake. These authors introduce an empirical nodal point boundary condition that controls the partitioning of water and sediment into the downstream branches. Their one-dimensional, steady, uniform flow analysis shows that the system contains only one stable state: a symmetrical division of discharge with both branches open. Slingerland and Smith [1998] improved on

Wang *et al.*'s model by using the one-dimensional St. Venant equations coupled with suspended sediment and Exner's equation for the case of river avulsions. They showed that symmetrical configurations are unstable to small perturbations. However, their analyses focused on conditions for avulsion and not exactly on bifurcation stability.

[10] In summary, our understanding of high  $\Theta$  bifurcations is severely limited. The current theoretical treatments are oversimplified and do not consider nonuniform flows that are known to be important in some bifurcations [Dargahi, 2004]. Current numerical treatments also rely on an artificial internal boundary condition, or nodal point relation, to distribute sediment at the bifurcation. A more sophisticated modeling approach that accounts for the effect of unsteady, nonuniform flow, and allows the system to develop its own nodal point relation is needed. Perhaps most importantly, field data are needed to validate the stability studies of high and low  $\Theta$  bifurcations.

[11] Given that high  $\Theta$  bifurcations are the dominant type on navigable rivers, there is a pressing need for detailed field data and improved theoretical modeling. To this end, our approach is to use numerical modeling to define the equilibrium solutions for high  $\Theta$  bifurcations and then perturb those configurations to see if they are stable. We then use field data to validate the predictions. Important objectives are: (1) to define the stability functions for high  $\Theta$  bifurcations and compare them to low  $\Theta$  bifurcations; (2) to define the hydraulic and sedimentary processes that create stable, asymmetrical, high  $\Theta$  channel bifurcations; and (3) to understand why bifurcating channels are generally asymmetrical with respect to their discharges, widths, and depths.

### 3. Numerical Model Description

#### 3.1. Model Description

[12] We model the processes within a fluvial-channel bifurcation using the computational fluid dynamics package Delft3D. Delft3D simulates fluid flow, waves, sediment transport, and morphological changes at timescales from seconds to years and has been validated for a wide range of hydrodynamic, sediment transport, and scour and deposition applications in rivers, estuaries, and tidal basins [Hibma *et al.*, 2004; Lesser *et al.*, 2004; Marciano *et al.*, 2005; Van Maren, 2005]. The equations of fluid and sediment transport and deposition are discretized on a curvilinear finite difference grid and solved by an alternating direction implicit scheme. An advantage of Delft3D is that the hydrodynamic and morphodynamic modules are fully coupled; the flow field adjusts in real time as the bed topography changes.

#### 3.2. Governing Equations

[13] Delft3D solves the three-dimensional nonuniform, unsteady, incompressible fluid flow Reynolds equations under the shallow water and Boussinesq assumptions. The equations consist of conservation of momentum, conservation of mass, and the transport equation. The vertical eddy viscosities are defined using a  $\kappa$ - $\epsilon$  turbulence closure scheme and the horizontal eddy viscosities are defined using a horizontal large eddy simulation that relates the horizontal fluid shear stress to the horizontal flow velocities. We did numerical experiments with and without the horizontal large eddy simulation and found it did not have an

appreciable effect on the final solutions. Therefore to reduce computational time, the horizontal large eddy simulation was not used and the horizontal fluid eddy diffusivities in all experiments are set to a constant value of  $0.0001 \text{ m}^2/\text{s}$  in the  $x$  and  $y$  directions. All results presented here use the vertically integrated two-dimensional equation set in Delft3D because the equilibrium solutions vary little from the three-dimensional solutions (5 equally sized computational layers in the vertical) by only a maximum of 15% of the equilibrium discharge ratio.

[14] Delft3D has separate mathematical treatments for the erosion and deposition of cohesive and noncohesive sediment. Cohesive sediment is defined as silt-sized and finer, whereas noncohesive sediment is defined as sand-sized and coarser. The formulation for cohesive sediment erosion and deposition is based on work by Partheniades [1965] and Krone [1962], whereas the formulation for noncohesive sediment erosion and deposition is based on the Shields curve.

[15] Cohesive and noncohesive sediment can be transported as bed load or suspended load depending on the grain size and the flow strength. Bed load transport rate per unit width is calculated from van Rijn [1984]. The magnitude and direction of the bed load transport vector is adjusted for favorable and adverse longitudinal slopes according to Bagnold [1966] and for transverse slopes according to Ikeda [1982]. Suspended load transport rate is calculated by solving the vertically integrated three-dimensional diffusion–advection equation, where the sediment eddy diffusivities are a function of the fluid eddy diffusivities. Gradients in the sediment transport vectors are used to determine changes in bed topography using the Exner equation. For a more detailed discussion on the mathematics of Delft3D and the flow/topography interactions, see Lesser *et al.* [2004].

### 4. Numerical Modeling Approach

#### 4.1. Model Grid Considerations

[16] For our experiments, we designed a computational grid with a straight unbifurcated (upstream) reach and two bifurcate reaches (Figure 2A). The unbifurcated reach is defined as channel  $a$ , the bifurcate channel with the smaller discharge is channel  $b$ , and the bifurcate channel with the larger discharge is channel  $c$ . The grid is perfectly symmetrical about the centerline of the unbifurcated reach with a bifurcation angle between the two bifurcate channels of  $55^\circ$ . The channels have fixed walls and the top width of each bifurcate is approximately one-half the width of the unbifurcated channel.

[17] Each bifurcate channel has a nondimensional length ( $L'$ ) of approximately 12.5 which is consistent with the average  $L'$  of approximately 14 reported by Edmonds *et al.* [2004] from a survey of 24 distributary deltas throughout the world.  $L'$  is defined as  $L' = L/W$ , where  $L$  is the dimensional channel length and  $W$  is the dimensional channel width. We did additional experiments with numerical grids that have longer bifurcate channels ( $L' = 37.5$ ) to see if  $L'$  influenced our results. Equilibrium solutions for the longer bifurcate channels fall within 6 to 10% of the equilibrium solution for shorter bifurcate channels, leading us to conclude that the results presented here are insensitive

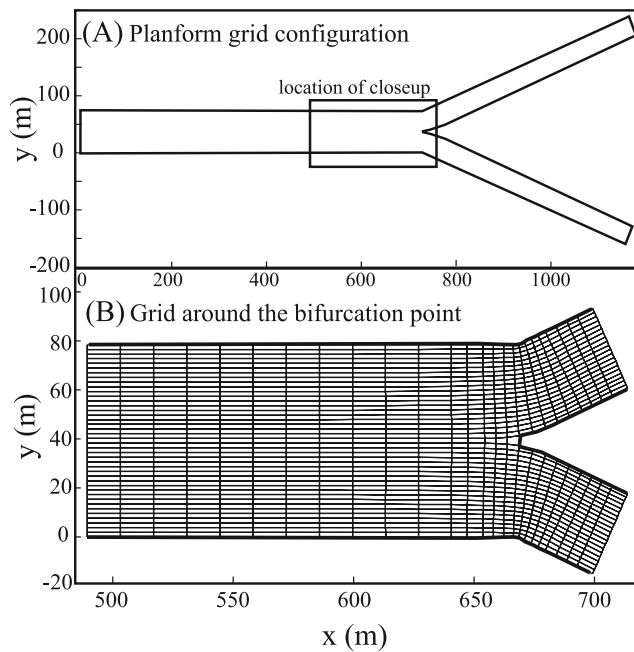


**Figure 2.** (A) Planform outline of numerical grid used in this study. (B) Close-up of the numerical grid showing individual cells. Each grid cell is approximately 2-m wide and 15-m long.

to the range of  $L'$  measured by *Edmonds et al.* [2004]. In all cases our channel lengths are shorter than the backwater length scale ( $\sim 15$  km for these experiments) as would be expected for distributary channels near the coastline.

[18] Numerical results should also be independent of grid cell size [*Hardy et al.*, 2003]. We tested for grid independence and found that the results of this study were relatively insensitive to grid size. Therefore we chose a grid that is numerically efficient yet still resolves topographic details in the evolving system. Each grid cell is a rectangle that is approximately 2-m wide and 15-m long with the long axis of the rectangle parallel to the flow direction. The time step in our experiments obeys the Courant–Frederichs–Levy criterion, and therefore the smallest cell determines the size of the maximum time step.

[19] Grids in Delft3D should be smooth and each cell should be orthogonal in order to conserve mass and momentum. To achieve orthogonality around the bifurcation point (Figure 2B), extra grid cells were added and an orthogonal transformation was applied using the Delft3D gridding software. The computational grid used in these experiments has a maximum deviation from orthogonality of  $20^\circ$ . This orthogonality does not affect the solution; experiments with higher orthogonality achieved results similar to results with lower orthogonality.

#### 4.2. Model Setup and Boundary and Initial Conditions

[20] The variables thought to govern the behavior of bifurcations can be grouped into three dimensionless parameters: Shields number of the unbifurcated reach,  $\Theta_a$ , aspect ratio of the unbifurcated reach,  $\alpha_a$ , and friction factor of the system,  $C'$ , where

$$\alpha = \frac{W}{D} \quad (2)$$

$W$  is the width (m) and  $D$  is the depth (m) and

$$C' = \frac{C}{\sqrt{g}} \quad (3)$$

$C$  is the dimensional Chezy roughness ( $\text{m}^{1/2}/\text{s}$ ), and  $g$  is the acceleration due to gravity ( $\text{m}/\text{s}^2$ ).

[21] The numerical modeling experiments use a range of these parameters to accurately represent fine-grained, cohesive fluvial bifurcations. The experiments are two-dimensional vertically integrated with one inlet and two outlets. The inlet boundary condition of channel  $a$  is a steady, uniform discharge across the channel carrying an equilibrium sediment concentration. The outlet boundary conditions are steady, uniform free water surface elevations for channel  $b$  ( $h_b$ ) and for channel  $c$  ( $h_c$ ). The bed elevations at the downstream boundaries are allowed to adjust during the simulations.

[22] At the inlet we prescribe equilibrium sediment concentrations that consist of a cohesive fraction of mud and a noncohesive fraction of fine-grained sand. Initially in the erodable substrate there is an equal proportion of evenly mixed noncohesive and cohesive sediment. We used a temporally and spatially invariant nondimensional Chezy roughness ( $C'$ ) value of 12.5 and the aspect ratio ( $\alpha$ ) of channel  $a$  of approximately 16 for all runs.  $\Theta_a$  varied from approximately 0.047 to 30.

[23] The initial river bed topography for each numerical experiment consists of a uniform bed elevation in each channel where the initial bed elevation in channel  $b$  is always higher than  $a$  and  $c$ . If there is a vertical offset between channel  $a$  and  $b$  (that is, if there is a vertical step at the entrance to channel  $b$ ) the model will not find an equilibrium solution because the local water surface slope induced by the offset causes channel  $c$  to capture all the flow. However, if there is no vertical offset and the entrance is sufficiently smooth the model is not sensitive to initial conditions. To generate a smooth entrance we construct a bed ramp by linearly interpolating the bed elevation from channel  $b$  approximately one or two multiples of  $W_a$  upstream [*Bolla Pittaluga et al.*, 2003]. This initial condition permits a variety of different bed ramp configurations that will evolve to a single equilibrium solution (Figure 3). The experiments in this study used the bed ramp configuration in Figure 3 that extends approximately 2 channel widths upstream from the bifurcation point.

#### 4.3. Obtaining an Equilibrium Bifurcation Configuration

[24] What is the appropriate metric for determining if a deltaic bifurcation is at equilibrium? Equilibrium deltaic systems are net depositional because the downstream boundary is changing due to delta progradation or changing sea level. However, as a first approximation we argue that we can assume that equilibrium deltaic bifurcations are adjusted for sediment bypass because the timescale for channel adjustment is very small compared to delta progradation. Therefore we follow the definition of *Miori et al.* [2006]; bifurcations are in equilibrium if they do not change

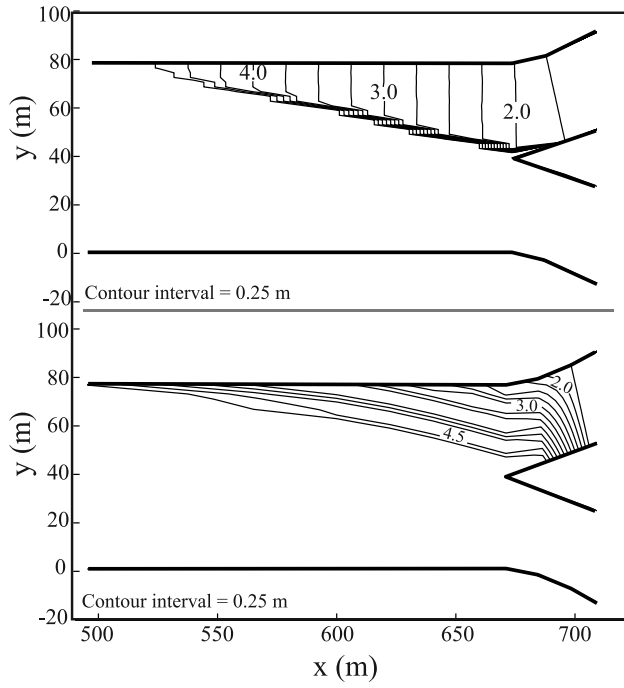


**Figure 3.** Two different initial bed ramp configurations tested in this study. In each configuration the bed elevation is contoured and is measured relative to the downstream boundaries of the bifurcate channels which are both zero. The results of this study are insensitive to the initial bed ramp configuration; therefore the top configuration was used. The location of the close-up is given in Figure 2A.

in morphology over some multiple of the morphological timescale ( $T_m$ ), where

$$T_m = \frac{W_a D_a}{q_{sa}} \quad (4)$$

$W_a$  is width (m) in channel  $a$ ,  $D_a$  is the depth (m) in channel  $a$ , and  $q_{sa}$  is the sediment transport rate per unit width ( $\text{m}^2/\text{s}$ ) in channel  $a$ .  $T_m$  is the duration over which the amount of sediment needed to fill a cross-section is transported through that cross-section. We consider a bifurcation to be in equilibrium if there is suspended and bed load transport in all reaches and the change in discharge ratio,  $Q_r$ , with time varies by no more than 1% around the equilibrium value for at least 15 multiples of nondimensional time ( $T_{ND}$ ), where

$$Q_r = \frac{Q_c}{Q_b}, \quad \text{and} \quad (5)$$

$$T_{ND} = \frac{T}{T_m} \quad (6)$$

$Q_c$  and  $Q_b$  are the water discharges ( $\text{m}^3/\text{s}$ ) in the channels with the larger and smaller water discharges, respectively,  $T$  is the total time elapsed and  $T_{ND}$  is the nondimensional time, or the multiples of the morphological timescale elapsed during the computation.

[25] To find equilibrium configurations in Delft3D we start with generic bed bathymetry with  $D_r \neq 1$ , where  $D_r$  is

the initial average depth ratio of the bifurcate channels, and a generic bed ramp between the channel  $b$  and channel  $a$ . We then adjust the Shields stress in channel  $a$  ( $\Theta_a$ ) until we find the value that produces an equilibrium bifurcation configuration from that set of boundary conditions and initial  $D_r$  (Figure 4) if one exists. We use this method to find the equilibrium solution because the nonlinear nature of the equations demands that the initial and boundary conditions be close to the solution for the model to recover that solution. As such, if the initial  $\Theta_a$  in Figure 4 is much larger than the equilibrium value,  $Q_r$  goes to 1, and if the initial  $\Theta_a$  is much smaller than the equilibrium value,  $Q_r$  goes to infinity, that is, one channel closes completely. The bold line in Figure 4 represents a single equilibrium bifurcation solution. To build an entire equilibrium diagram we chose a number of different initial  $D_r$  values and found the corresponding  $\Theta_a$  that resulted in an equilibrium bifurcation.

[26] Delft3D allows the user to speed up the bed adjustments by multiplying the deposition or erosion rate in each time step by a morphological scale factor. A series of sensitivity experiments showed that the final solution is insensitive to a morphological scale factor less than 250. We used a factor of 50. Approximately 100 simulations were conducted to define an equilibrium field.

## 5. Results

[27] There are two classes of equilibrium bifurcations, those which have equal water surface elevations at their downstream boundaries, such as bifurcations on deltaic coasts (Figure 1), and those which have an imposed advantage due to different water surface slopes, such as more mature bifurcations farther up delta. The differences between the equilibrium states of each class are not well defined. To this end, we conducted two sets of equilibrium experiments, one with equal water surface elevations at the outlets of channels  $b$  and  $c$  ( $h_b = h_c$ ) and one with an imposed water surface slope advantage from unequal water surface elevations at the outlets of channels  $b$  and  $c$  ( $h_b \neq h_c$ ). Delft3D finds symmetrical ( $D_r$  and  $Q_r = 1$ ) and asymmetrical ( $D_r$  and  $Q_r \neq 1$ ) equilibrium functions for both experiment sets. We first present a description of the typical equilibrium bifurcation with a symmetrical and asymmetrical configuration common to both experiments. Then we summarize the results from all experiments in a bifurcation equilibrium diagram and comment on the stability of the equilibrium solutions.

### 5.1. Description of the General Bifurcation Equilibrium Configuration

[28] The equilibrium bifurcations created in this study share the same basic topographic and hydraulic forms and features: (1) across the entrances to channels  $b$  and  $c$  there is cross-channel variation of water surface elevation and bed topography (Figure 5); (2) there is a positive bed ramp at the entrance to channel  $b$  and a negative bed ramp at the entrance to channel  $c$  (Figure 5); (3) the thalwegs for channels  $b$  and  $c$  are located on their southern and northern banks, respectively (Figure 5); and (4) in equilibrium asymmetrical configurations, the water surface topography is complex around the bifurcation point (Figure 6).

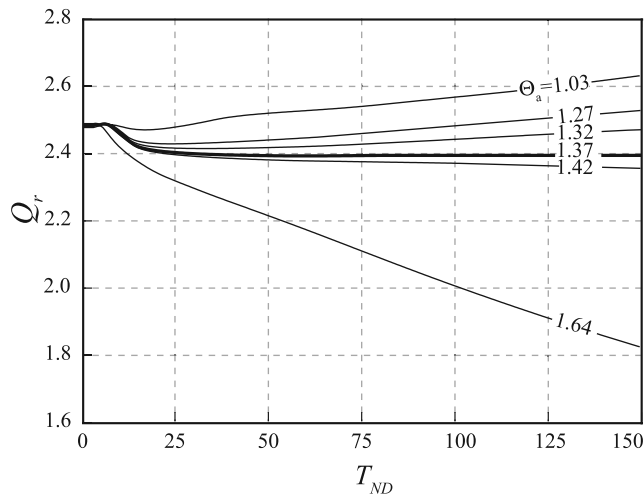


**Figure 4.** Evolution of the discharge ratio for different initial  $\Theta_a$ . The initial conditions are generic bed and water surface topography at  $T_{ND}$  equals 0. The bold line is an invariant  $Q_r$  over many  $T_{ND}$  and is considered to be an equilibrium solution for that set of boundary conditions. Variables defined in text and nomenclature list.

[29] The cross-channel variations in water surface elevation and bed topography at the entrances to channels  $b$  and  $c$  are the result of the interaction of the flow with an obstruction (i.e., the point of the bifurcation and the bed ramp). This can be understood by considering a streamline through the middle of channel  $a$  that intersects the bifurcation point of a symmetrical bifurcation ( $D_r$  and  $Q_r = 1$ ). If energy along that streamline is conserved, the water surface must rise because kinetic energy is converted to potential energy at the bifurcation point where the velocity goes to zero. In our experiments we observe a rise in water surface of 0.5 to 1 cm (point a in Figure 5A), which is similar to the 1 to 2 cm rise predicted by the Bernoulli equation. Additionally, streamlines just north and south of the bifurcation point respond similarly to the bifurcate channel curvature and the water surface is also elevated (point a in Figure 5A). The elevated water surface around the bifurcation point creates a low velocity zone at the bifurcation point and in turn sediment is deposited in the entrances to channels  $b$  and  $c$  (point c in Figure 5A). If at the entrances to channels  $b$  and  $c$  part of the water surface is elevated and the corresponding velocity is low, to conserve mass through the entire cross section, part of the water surface must also be depressed (point b in Figure 5A) and the local velocity increased on the outside bank. The higher velocity produces scour holes (point d in Figure 5A) on the northern and southern banks at the entrances to channels  $b$  and  $c$ , respectively.

[30] Now consider a streamline that intersects the bifurcation point in an asymmetrical bifurcation ( $D_r$  and  $Q_r \neq 1$ ; Figure 5B). The same general water surface and topographic forms described above are observed. However, the bed ramp is more effective at increasing the water surface elevation because in addition to conversion of kinetic to potential energy due to the obstruction of the bed ramp, the water surface is also elevated due to the increasing elevation of the bed. The presence of the bed ramp makes the elevated water surface asymmetrical in the entrances to channels  $b$

and  $c$  (point a in Figure 5B). This also creates asymmetrical bed topography (point d in Figure 5B) that is a skewed version of the symmetrical case. At equilibrium the bed ramps of both channels extend  $0.9W_a$  to  $2.25W_a$  upstream from the bifurcation point at low and high equilibrium values of  $Q_r$ , respectively (e and f in Figures 5A, 5B).

[31] The bifurcate thalwegs are located on the northern and southern banks of channels  $b$  and  $c$  respectively (g in Figures 5A and 5B), because upstream of the bifurcation fluid parcels in channel  $a$  have a momentum vector oriented parallel to the banks of channel  $a$ . As those fluid parcels enter channels  $b$  and  $c$  they are not immediately aligned with the banks of channels  $b$  and  $c$ . The inherited momentum orientation from channel  $a$  forces the high velocity thread to the southern and northern banks of channels  $b$  and  $c$ , respectively. In turn, this causes the thalweg downstream of the bifurcation point to be located in the same position (g in Figures 5A and 5B).

[32] In an equilibrium asymmetrical bifurcation the water surface elevation profiles down the middle of channels  $b$  and  $c$  are nonuniform; the water surface at the entrance to channel  $b$  is elevated, while at channel  $c$  it is depressed relative to a uniform water surface slope (Figure 6). The nonuniformity of the water surface extends upstream  $2.5W_a$  to  $5W_a$  at low and high equilibrium values of  $Q_r$ , respectively. The cause of the nonuniform water surface configuration around the bifurcation is related to flow past an obstruction and the presence of a bed ramp in each channel.

[33] The morphodynamic feedbacks among the dynamic water surface elevation, flow velocities, bed slopes, and sediment transport vectors create an equilibrium bifurcation in which  $Q$  and sediment discharge ( $Q_s$ ) of the bifurcate channels are delicately adjusted to just transport the sediment and water delivered to them. In this example (Figure 5 and Figure 6) the ratios are  $Q_r$  and  $Q_{s,r} \approx 2.5$ .

## 5.2. Equilibrium Diagram

[34] Similar to the theoretical analysis of coarse-grained bifurcations [Bolla Pittaluga *et al.*, 2003; Miori *et al.*, 2006], our equilibrium diagram for fine-grained, cohesive bifurcations is characterized by three equilibrium functions in  $\Theta_a$  space: (1) at all values of  $\Theta_a$  above transport and with  $h_b = h_c$ , there is an equilibrium function with  $D_r$  and  $Q_r = 1$  (Figure 7A); (2) at relatively low values of  $\Theta_a$  and with  $h_b = h_c$ , there is an equilibrium function with  $D_r$  and  $Q_r \neq 1$  (Figure 7B); and (3) at relatively high values of  $\Theta_a$  and with  $h_b \neq h_c$ , there is an equilibrium function with  $D_r$  and  $Q_r \neq 1$  (Figure 7C). The symmetrical equilibrium function occurs through all values of  $\Theta_a$  greater than the critical Shields stress,  $\Theta_{crit}$  (Figure 7A). This is an unsurprising result and has also been found with other numerical models [Wang *et al.*, 1995; Slingerland and Smith, 1998].

[35] More surprisingly, at  $\Theta_a < 2.3$  and  $h_b = h_c$  there are asymmetrical equilibrium bifurcations, whose equilibrium  $Q_r$  is a positive function of  $\Theta_a$  (Figure 7B). The function stops at  $Q_r > 6.5$  because  $Q_b$  becomes so small that  $\Theta_b$  falls below  $\Theta_{crit}$  for noncohesive sediment. Delft3D predicts that  $Q_r$  increases (becomes more asymmetrical) as  $\Theta_a$  increases, which is opposite to predictions for coarse-grained bifurcations determined using numerical solutions of the steady, uniform flow equations [Bolla Pittaluga *et al.*, 2003; Miori *et al.*, 2006] and flume experiments [Bertoldi and Tubino, 2007].

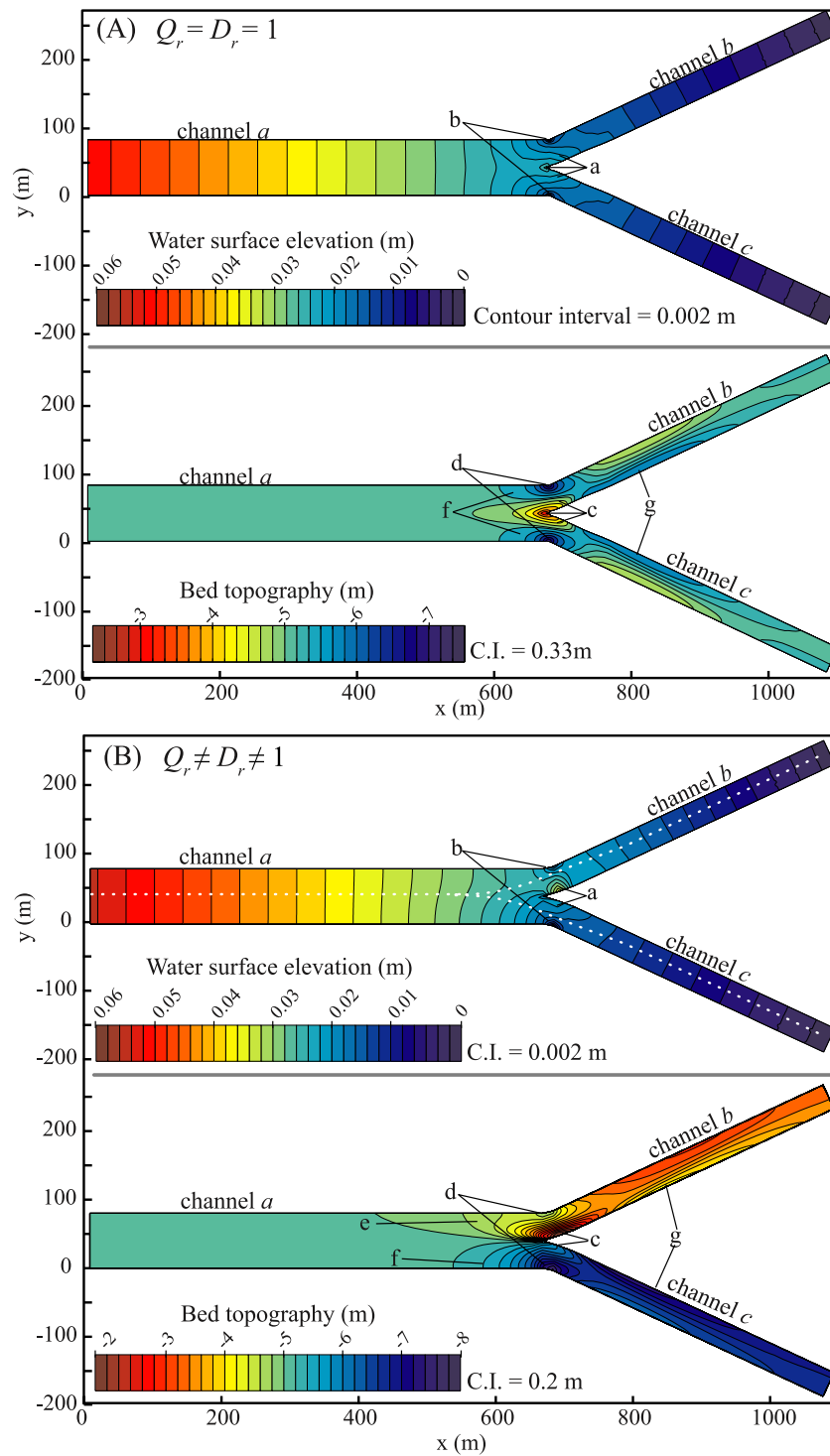


**Figure 5.** (in color) Examples of symmetrical (A) and asymmetrical (B) water surface elevation and bed topography at equilibrium as computed by Delft3D. The solutions have the following characteristics: (1) at the entrances to channels *b* and *c* there are regions of the water surface that are elevated (a) and depressed (b) and topographic features of positive (c) and negative (d) relief; (2) there is a positive bed ramp (e) at the entrance to channel *b* and a negative bed ramp (f) at the entrance to channel *c*; and (3) the channel thalwegs (g) of channels *b* and *c* are located along the southern and northern banks, respectively. The bed topography is measured with respect to the downstream water surface elevation boundary, which is zero in these cases. The white dotted lines in (B) refer to locations of water surface elevation profiles in Figure 6. In this example  $Q_a = 257.5$ ,  $Q_b = 75$ , and  $Q_c = 182.5$ . For a more detailed explanation, see section 5.1.

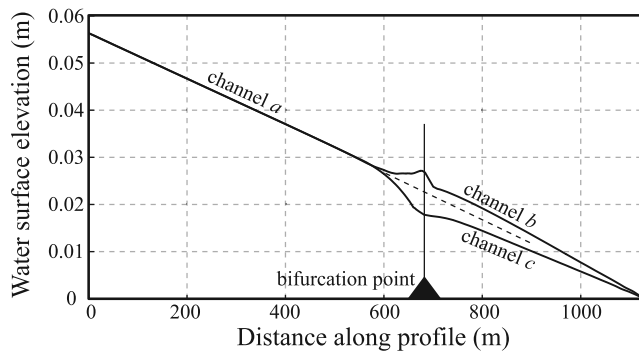


**Figure 6.** Equilibrium water surface profiles for an asymmetric bifurcation. The profile of channel *b* is elevated, while the profile of channel *c* is depressed relative to a uniform slope (black dashed line). The elevation and depression extend well upstream of the bifurcation (solid triangle). The locations of the profiles correspond to the while dotted lines in Figure 5.

[36] Why does Delft3D predict an increase in equilibrium  $Q_r$  with increasing  $\Theta_a$ ? We computed the static flow and sediment transport fields at various values of  $Q_r$  (or bed ramp height) while holding  $\Theta_a$  constant. The bed was not allowed to deform. An increase in bed ramp height ( $\eta$ ) causes an increase in  $Q_r$  and sediment discharge ratio,  $Qs_r$  ( $m^3/s$ ), because more discharge and sediment are diverted to channel *c* than to channel *b* by the larger  $\eta$ . An increase in  $\eta$  also increases the water surface slope in channel *b* (Figure 8). A steeper water surface slope in channel *b* requires more bed load to be delivered to the entrance of channel *b* to remain in equilibrium, and this can only happen if  $\Theta_a$  is larger. The result is a counterintuitive, inverse relationship between water and bed load discharge (Figure 9) in the smaller discharge channel of equilibrium bifurcations, because an increase in  $Q_r$  simultaneously causes an increase in water surface slope (and hence bed load transport) and a decrease in discharge of that channel. Therefore the trend of this equilibrium function is a conse-

quence of the elevated and depressed water surface (Figures 6 and 8) around the bifurcation point that allows for equilibrium asymmetrical energy slopes and sediment transport rates in the bifurcate arms.

[37] At  $\Theta_a > 2.1$  with  $h_b \neq h_c$ , Delft3D predicts that equilibrium  $Q_r$  decreases as  $\Theta_a$  increases for a given combination of  $h_b$  and  $h_c$  (Figure 7C). For this particular realization the initial depth in channels *b* and *c* are equal, and  $h_c$  was set 2.5 mm lower than  $h_b$ , which makes the water surface slope in channel *c* 10% steeper than channel *b*. The lowest  $\Theta_a$  for which this equilibrium solution exists depends on the  $h_c/h_b$  ratio. As  $\Theta_a$  increases, the equilibrium  $Q_r$  approaches 1 asymptotically. This occurs because the slope advantage imposed by different  $h_b$  and  $h_c$  becomes an increasingly small percentage of the water surface slope at high  $\Theta_a$ . Nonetheless, it is interesting that the asymmetrical function with  $h_b \neq h_c$  does not exist for all values of  $\Theta_a$ . This function terminates at low  $\Theta_a$  because the water surface slope down the favored bifurcate arm is steep compared to the water surface slope in channel *a*, and all the sediment and discharge are routed down the favored bifurcate channel. Thus for each realization of  $h_b \neq h_c$ , there is a threshold point in  $\Theta_a$  space below which the water surface slope ratio between the unbifurcated reach and the favored bifurcate reach is too large to maintain an equilibrium asymmetrical solution.

### 5.3. The Effect of Changing Channel Roughness ( $C'$ ) and Aspect Ratio of Upstream Channel ( $\alpha_a$ ) on the Equilibrium Functions

[38] It is important to remember that the results presented so far are for a particular combination of  $\alpha_a$  and  $C'$ . Additional numerical experiments show that at larger (smaller) values of  $\alpha_a$  the relatively low  $\Theta_a$  equilibrium function (Figure 7B) shifts to a higher (lower) equilibrium  $Q_r$  for a given  $\Theta_a$ . At larger (smaller) values of  $C'$  the relatively low  $\Theta_a$  equilibrium function (Figure 7B) shifts to a lower (higher) equilibrium  $Q_r$  for a given  $\Theta_a$ . At larger (smaller) values of  $\alpha_a$  the relatively high  $\Theta_a$  equilibrium function (Figure 7C) shifts to a lower (higher) equilibrium

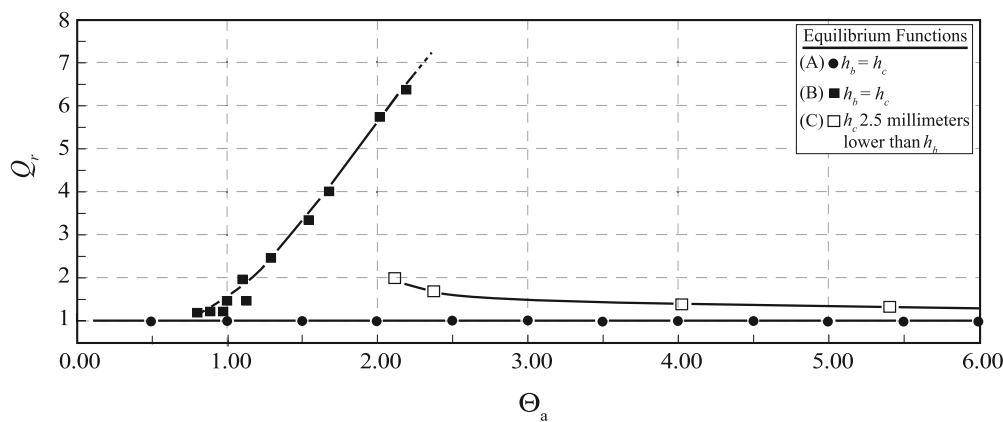


**Figure 7.** Equilibrium diagram for fine-grained, cohesive deltaic bifurcations. The bold lines are inferred continuous equilibrium solutions. (A) Equilibrium symmetrical solution with  $h_b = h_c$  occupies all values of  $\Theta_a > \Theta_{crit}$ . (B) Equilibrium asymmetrical solution ( $Q_r \neq 1$ ) with  $h_b = h_c$  terminates at  $\Theta_a \sim 7$  because  $\Theta_b < \Theta_{crit}$ . (C) Equilibrium asymmetrical solution with  $h_b \neq h_c$  approaches 1 as  $\Theta_a$  approaches  $\sim 30$ . This particular solution has  $h_c$  2.5 mm lower than  $h_b$ . All equilibrium solutions are computed for  $\alpha_a = 16$  and  $C' = 12.5$ . Each equilibrium function also exists for the inverse of  $Q_r$ .

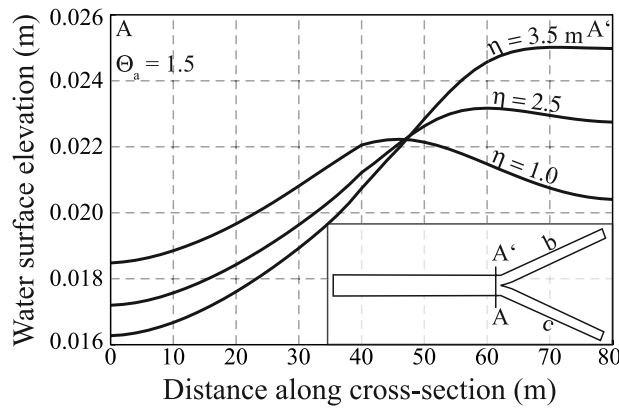


**Figure 8.** For a given  $\Theta_a$ , an increase in bed ramp height ( $\eta$ ) increases the water surface at the entrance to channel  $b$ . The water surface elevation is relative to  $h_b$  and  $h_c$  (which are equal).

$Q_r$  for a given  $\Theta_a$ . At larger (smaller) values of  $C'$  the relatively high  $\Theta_a$  equilibrium function (Figure 7C) shifts to a higher (lower) equilibrium  $Q_r$  for a given  $\Theta_a$ .

#### 5.4. Are These Equilibrium Configurations Stable to Perturbations?

[39] To test if the equilibrium configurations are stable we added a perturbation to the equilibrium river bed topography and let the model continue to compute forward. If the perturbation was damped and the bifurcation returned to the original equilibrium form then that configuration is considered to be in a stable equilibrium. We follow previously published methodology [Bolla Pittaluga *et al.*, 2003] and add a small sediment bump ( $\sim 50$  cm high and  $10500$  cm<sup>3</sup> or approximately a 5–10% net change in channel cross-sectional area) in the middle of channel  $b$ .

[40] All three equilibrium functions (Figure 7) are stable to small perturbations; when subjected to a perturbation in the shallower bifurcate channel the system returns to the equilibrium configuration (Figure 10). Additional numerical experiments prove that all configurations in the three equilibrium functions are stable to a small sediment bump in the middle of channel  $b$ . However, if the size of that sediment bump is sufficiently large ( $\sim 100$  cm high and  $450,000$  cm<sup>3</sup> or a 30–40% net change in channel cross-sectional area), the symmetrical configuration is no longer stable. This is true for all symmetrical solutions over the range of  $\Theta_a$  in Figure 7. For example, if the symmetrical equilibrium solution with  $Q_r = 1$  and  $\Theta_a = 1$  is perturbed with a large sediment bump the new equilibrium solution has  $Q_r = 1.1$ . These results suggest that asymmetrical bifurcations are more stable to perturbations compared to symmetrical bifurcations.

## 6. Validation of Model Results Using Field Data

[41] To validate the theoretical predictions [in the sense of Hardy *et al.*, 2003] we collected river bed topography, hydraulic data, and water surface elevations on eight natural bifurcations in the Mossy delta, Saskatchewan, Canada (Figure 1A). River bed elevations were collected using an EAGLE FishElite 500c single-beam echo sounder. Channel water discharges were measured with an acoustic Doppler

current profiler at near bankfull flow stage (Parsons and Best, personal communication). Water surface elevation data were collected by mounting a Leica differential global positioning system (dGPS) rover (receiver) in a boat floating down the middle of the channels recording water surface elevations every second. The elevation data were processed with Ski-Pro v. 3.0 using a base station of known elevation. This technique is advantageous because the high temporal resolution and vertical accuracy resolve the details of the water surface. To validate this technique, we floated the same river reach multiple times over different days and observed the features of water surface topography in each float.

[42] The value of  $\Theta_a$  for each bifurcation was calculated using measured bed grain sizes, water surface slopes, and channel geometries. Time series of channel geometry for most bifurcations indicate that their widths have adjusted in accord with hydraulic geometry scaling [Edmonds, unpublished data], suggesting that Mossy delta bifurcations are in equilibrium with the flow field. Additionally, a serial aerial photographic analysis shows most bifurcations have been active for over 35 years [Oosterlaan and Meyers, 1995; Edmonds and Slingerland, 2007], and have not changed appreciably in planform. Thus we take the Mossy delta bifurcations to be stable, equilibrium forms and if the predictions of Delft3D are accurate these forms should compare favorably with the theoretical numerical modeling results.

[43] The river beds and water surfaces of Mossy delta bifurcations are similar to the stable, equilibrium forms predicted in this study (cf. Figures 2 and 11). The river beds of the natural bifurcations have the same topographic features as the stable, equilibrium bifurcations produced in Delft3D (e.g., Figure 5). Additionally, the water surface profiles of Mossy delta bifurcations show elevated and depressed topographic configurations near the bifurcation similar to model predictions (Figure 12). The water surface is elevated at bifurcation points producing steeper water surface slopes in two-thirds of the lower discharge bifurcate channels ( $n = 8$ ), indicating that the nonuniform water surface is a common feature in natural bifurcations.

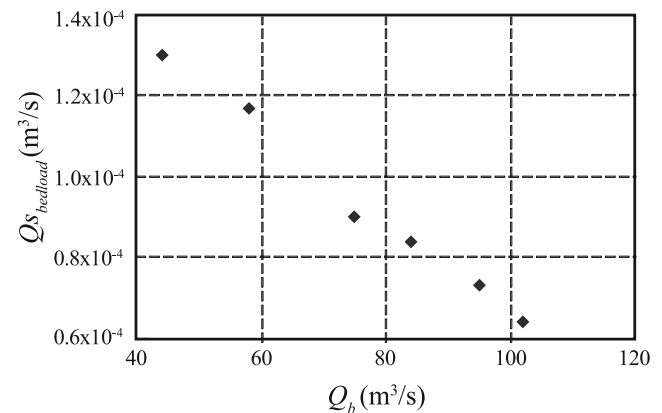


**Figure 9.** In equilibrium bifurcations computed in this study there is an inverse relationship between bed load transport ( $Q_{s_{bedload}}$ ) in channel  $b$  and discharge ( $Q_b$ ) in channel  $b$ . See text for details.

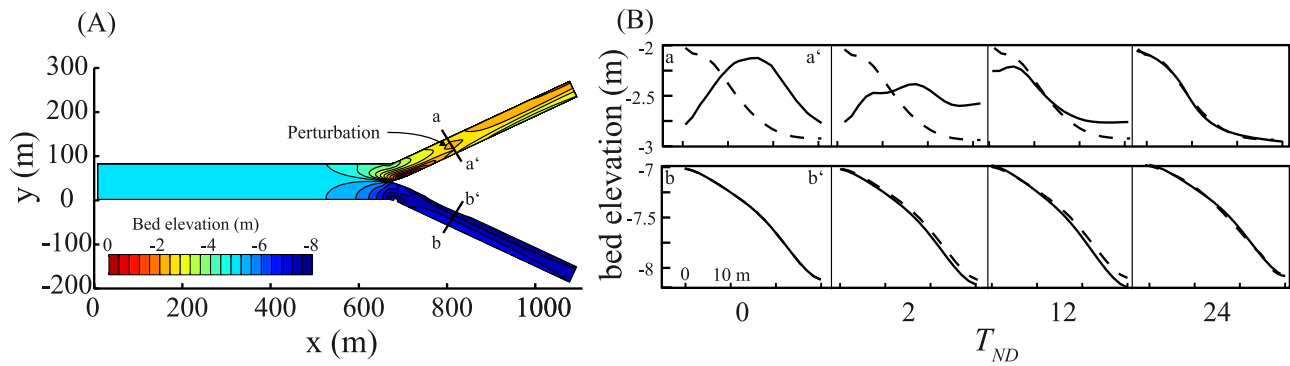


**Figure 10.** Evolution of a perturbed equilibrium bed. (A) Bed topography at equilibrium is perturbed by adding a mound of sediment in the middle of the channel (see section a-a') in channel b. (B) Channel cross-sections along a-a' (top) and b-b' (bottom) through time showing the equilibrium bed (dotted line) and evolving bed (solid line). The perturbed bed returns to the equilibrium morphology after  $T_{ND} = 24$ .

[44] The eight Mossy delta bifurcations generally plot on or near the equilibrium function in the stability diagram and exhibit a trend similar to theory (Figure 13). We take the favorable comparisons between predicted and observed bed topographies (Figure 11), water surface topographies (Figure 12), and locations on the theoretical stability diagram (Figure 13) as support for the stability diagram.

## 7. Discussion

### 7.1. Comparison to Previously Published Models

[45] The asymmetrical bifurcation stability function presented here (Figure 7B) is different from previously published results [Bolla Pittaluga *et al.*, 2003; Miori *et al.*, 2006; Bertoldi and Tubino, 2007]. For braided river bifurcations the stable, equilibrium  $Q_r$  decreases as  $\Theta_a$  increases. We think our stability solution has the opposite trend because the fine-grained, cohesive system is sensitive to, and controlled by, the strongly nonuniform water surface topography at the bifurcation. Our results were computed

for a high  $\Theta$  system and it is unknown if the previously published stability solutions at low  $\Theta$  will be as sensitive to the nonuniform water surface topography at the bifurcation.

[46] Asymmetrical bifurcations are stable in braided rivers because the bed ramp significantly alters the sediment transport vector [Bolla Pittaluga *et al.*, 2003], thereby allowing each bifurcate channel to receive different amounts of sediment due to the transverse sediment flux ( $Q_{ST}$ ) at the bifurcation point.  $Q_{ST}$  is defined as

$$Q_{ST} = Q_S - Q_S^*$$

where  $Q_S$  ( $m^3/s$ ) is the sediment flux in a bifurcate channel for a given solution and  $Q_S^*$  ( $m^3/s$ ) is the sediment flux in that bifurcate channel for an symmetrical bifurcation with the same hydraulic conditions. The difference is the sediment that is being redirected due to the presence of the bed ramp. Our results from Delft3D confirm that the effect of transverse slopes on the sediment transport vector

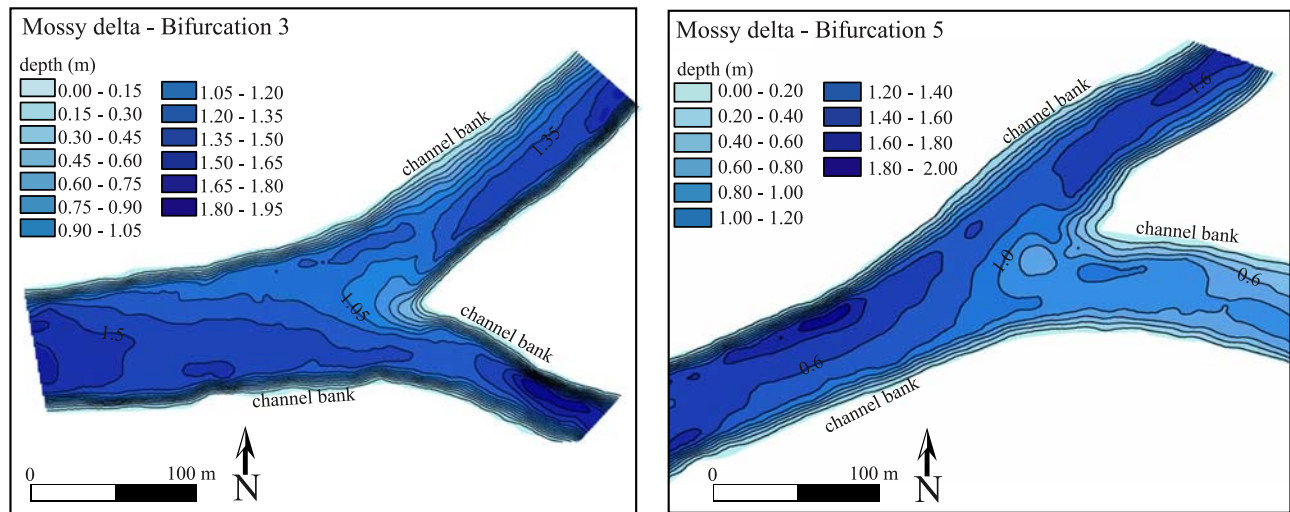


**Figure 11.** (in color) River bed topography of natural bifurcations on the Mossy delta, Saskatchewan, Canada. The locations of Mossy delta bifurcations are marked on Figure 1. These data were collected at near bankfull flow stage in July 2006. The natural bifurcations have features similar to equilibrium bifurcations produced in Delft3D. There are depositional and scour features around the bifurcation point, there is a positive bed ramp from the main channel to the shallower channel, and the bifurcate thalwegs are located on the inner banks.

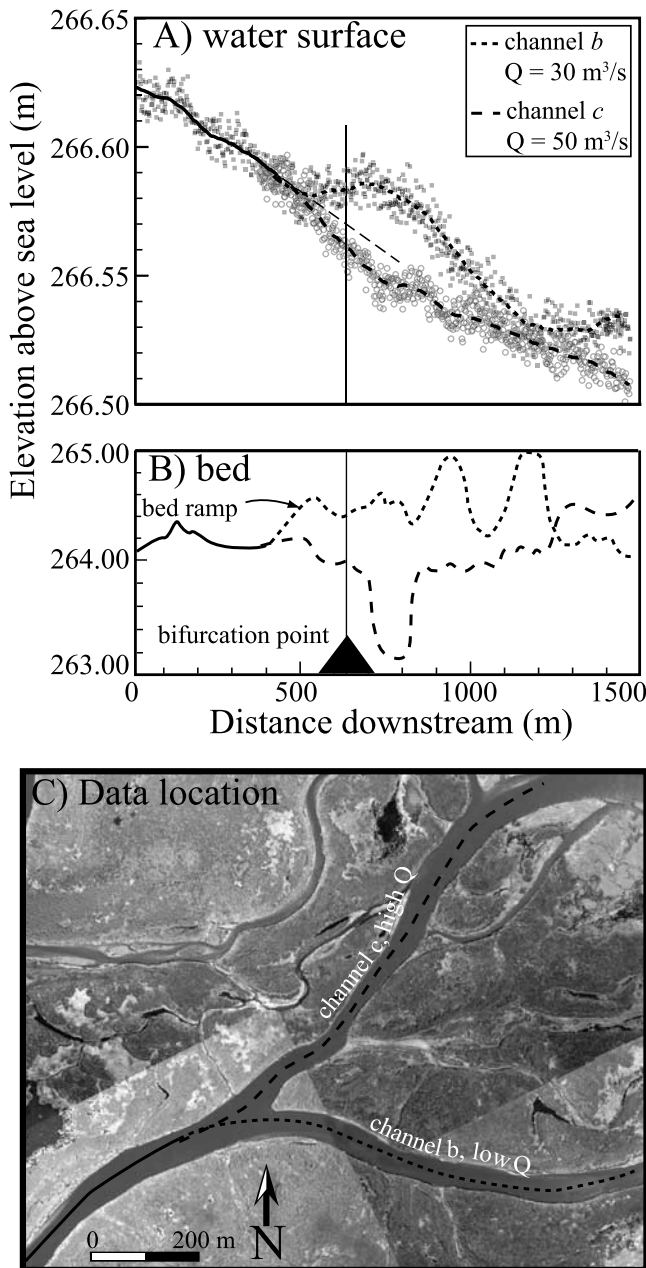


**Figure 12.** (A) Water surface elevations on a bifurcation taken with a Leica dGPS. Bold line is a 50-m running average. (B) River bed elevations taken with a single beam echo sounder. (C) Planview map of Mossy delta bifurcation number 5 (location in Figure 1) showing the locations of data track lines. Similar to Delft3D predictions, the channel with a lower  $Q$  and a bed step (channel  $b$ ) has an elevated water surface relative to the projected uniform water surface slope, while the channel with a higher  $Q$  (channel  $c$ ) has a depressed water surface.

is a necessary condition for achieving asymmetrical stability, but interestingly for fine-grained cohesive bifurcations it is not a sufficient condition. If the transverse slope effect on bed load transport is removed in our models,  $Q_{ST}$  changes by only a few percent. Rather, the dominant mechanism of sediment steering is topographic steering of flow and sediment trajectories due to the presence of the bed ramp and nonuniform water surface elevation at the

entrances of the two bifurcate channels. This topography at the bifurcation cannot be known *a priori*, instead it is the result of the morphodynamical feedbacks between a coevolving river bed and flow field.

## 7.2. Why are Deltaic Bifurcations Asymmetrical?

[47] As noted earlier, on average, deltaic bifurcations have asymmetrical widths, depths, and discharges in the bifurcate channels. Our results show that asymmetrical bifurcations are more stable to perturbations than symmetrical bifurcations. In addition, *Bertoldi and Tubino* [2007] recently proposed a novel explanation for bifurcation asymmetry that may also hold true for deltaic bifurcations. They noted that under super-resonant conditions, the presence of the bifurcation causes a transverse bed perturbation upstream that topographically steers more flow into one of the bifurcate channels.

[48] The prevalence of asymmetrical bifurcations in nature implies that there must be perturbations that drive the bifurcation away from symmetry. The results from this study (section 5.4) show that symmetrical bifurcations are less stable; a large perturbation can force the symmetrical bifurcation to become asymmetrical. There are a variety of perturbations that could cause bifurcation asymmetry ranging from process perturbations, such as the bifurcation itself [*Bertoldi and Tubino, 2007*], alternating side bars [*Miori et al., 2007*], and river meandering [*Kleinhans et al., 2008*], to white noise perturbations, such as floods, circulation dynamics in the standing body of water, water surface slope advantages, and planform advantages. Therefore we suggest that asymmetrical bifurcations are prevalent because a symmetrical bifurcation will eventually become asymmetrical due to myriad perturbations in nature. Once bifurcations are asymmetrical, the nonuniform water surface topography at the bifurcation and the effect of the bed ramp on the flow field provide feedbacks that keep asymmetrical bifurcations stable.

## 8. Conclusions

[49] We have attempted to explain the origin of asymmetrical bifurcations of river channels by investigating their

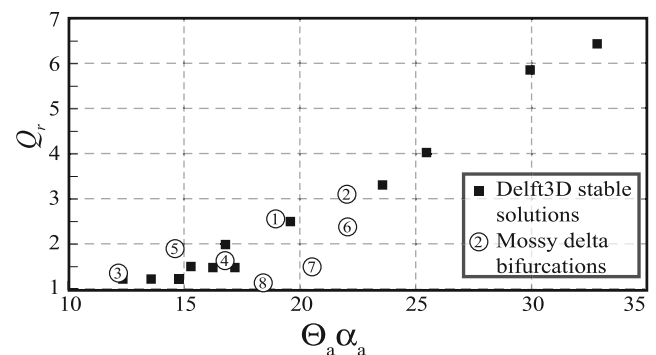


**Figure 13.** Stable bifurcations from the Mossy delta (see Figure 1 for locations) generally plot in the stable, equilibrium space predicted by Delft3D. We multiplied  $\Theta_a$  by  $\alpha_a$  to remove the effect of different aspect ratios among the natural bifurcations. The scatter in the field data is related to natural bifurcations having bifurcate channels of different widths and measurements of discharge and water surface slope taken at less than bankfull discharge.

stability using a two-dimensional vertically integrated morphodynamic numerical model (Delft3D). The morphodynamic feedbacks between the evolving bed and water surface create three distinct equilibrium functions where the equilibrium discharge ratio ( $Q_r$ ) is a function of the Shields stress in the unbifurcated reach ( $\Theta_a$ ). The first function has a symmetrical division of discharge in the bifurcate channels; the other two are asymmetric. With equal downstream water surface elevations (no imposed advantage for either channel), the stable, equilibrium  $Q_r$  becomes more asymmetrical as  $\Theta_a$  increases because the water surface elevation at the bifurcation rises, steepening the water surface slope, and thereby requiring a higher  $\Theta_a$  for equilibrium. For unequal downstream water surface elevations (imposed advantage for one channel) the equilibrium  $Q_r$  becomes more symmetrical as  $\Theta_a$  increases because at large  $\Theta_a$  the water surface slope advantage imposed by unequal downstream boundaries is a small percentage of the overall water surface slope.

[50] When subjected to a perturbation, such as a small sediment mound in a bifurcate channel, the asymmetrical bifurcations return to their equilibrium configuration whereas the symmetrical bifurcation moves to an asymmetrical stable equilibrium solution. Our results suggest that asymmetrical bifurcations are prevalent in nature because they are stable to a wider range of perturbations.

[51] These results are supported by field data from bifurcations of the Mossy delta in Saskatchewan, Canada. Field hydraulic geometry data and a 60-year history of little change suggest that the Mossy delta bifurcations are in stable equilibrium with their flow field. The Mossy delta bifurcations contain remarkably similar asymmetric bed geometries and water surface profiles to those predicted by Delft3D. Furthermore, when the Mossy delta bifurcations are plotted on the stability diagram they plot in stable space.

## Nomenclature Table

$C$	Chezy roughness, $L^{1/2} T^{-1}$
$C'$	nondimensional Chezy bed roughness
Channel $a$	the unbifurcated channel
Channel $b$	the bifurcate channel with the smaller discharge
Channel $c$	the bifurcate channel with the larger discharge
$D$	channel depth, L
$D_{50}$	median bed grain size, L
$D_r$	average depth ratio; high discharge channel divided by low discharge channel
$g$	acceleration due gravity, $L T^{-2}$
$h_b, h_c$	water surface elevations at the downstream boundaries of channels $b$ and $c$ , L
$L$	bifurcate channel length, L
$L'$	bifurcate channel length relative to the channel width
$Q$	water discharge, $L^3 T^{-1}$
$Q_r$	water discharge ratio; high discharge channel divided by low discharge channel
$q_s$	sediment transport rate per unit width, $L^2 T^{-1}$

$Q_s$	sediment transport rate, $L^3 T^{-1}$
$Q_s^*$	sediment transport rate in a symmetrical solution, $L^3 T^{-1}$
$Q_{s_{bedload}}$	sediment transport rate of the bed load fraction, $L^3 T^{-1}$
$Q_{s_r}$	sediment flux ratio; high discharge channel divided by low discharge channel
$Q_{s_T}$	transverse sediment flux at the bifurcation, $L^3 T^{-1}$
subscript $a, b, c$	refers to either channel $a, b$ , or $c$
$T_m$	morphological timescale, T
$T_{ND}$	nondimensional time
$W$	channel top-width, L
$x, y$	planform dimension, L
$\Theta$	Shields stress
$\Theta_{crit}$	critical Shields stress for incipient motion of a given sediment size
$\alpha$	channel aspect ratio; width divided by depth
$\eta$	bed ramp height, L
$\rho$	fluid density, $M L^{-3}$
$\rho_s$	sediment density, $M L^{-3}$
$\tau_o$	basal fluid shear stress $M L^{-1} T^{-2}$

[52] **Acknowledgments.** This research was done while D. A. Edmonds was supported by NSF grant EAR-0417877 awarded to R. L. Slingerland. Acknowledgement is also made to the donors of the American Chemical Society Petroleum Research Fund for partial support of this research. The authors would like to thank B. Jagers and M. G. Kleinhans for useful discussions about Delft3D. Additionally, we would like to thank J. L. Best, J. S. Bridge, D. Janesko, F. E. Klein, D. R. Parsons, A. R. Reesnik, and N. D. Smith for field support and useful discussions regarding deltas and their bifurcations. We are grateful to Chris Paola and two anonymous reviewers whose insightful comments strengthened this manuscript.

## References

- Andren, H. (1994), *Development of the Laitaure delta, Swedish lappland: A study of growth, distributary forms, and processes*, 188 pp., Uppsala University, Uppsala, Sweden.
- Ashmore, P. E., R. I. Ferguson, K. L. Prestegard, P. J. Ashworth, and C. Paola (1992), Secondary flow in anabranch confluences of a braided, gravel-bed stream, *Earth Surf. Processes Landforms*, 17, 299–311.
- Ashworth, P. J. (1996), Mid-channel bar growth and its relationship to local flow strength and direction, *Earth Surf. Processes Landforms*, 21, 103–123.
- Ashworth, P. J., R. I. Ferguson, P. E. Ashmore, C. Paola, D. M. Powell, and K. L. Prestegard (1992), Measurements in a braided river chute and lobe: 2. Sorting of bed load during entrainment, transport, and deposition, *Water Resour. Res.*, 28, 1887–1896.
- Axelsson, V. (1967), The Laitaure Delta: A study of deltaic morphology and processes, *Geogr. Ann. A: Phys. Geogr.*, 49(1), 127.
- Bagnold, R. A. (1966), An approach to the sediment transport problem from general physics, Professional Paper, pp. 11–137, Department of the Interior, USGS, Washington, D.C.
- Bertoldi, W., and M. Tubino (2005), Bed and bank evolution of bifurcating channels, *Water Resour. Res.*, 41, 1–12, W07001, doi:10.1029/2004WR003333.
- Bertoldi, W., and M. Tubino (2007), River bifurcations: Experimental observations on equilibrium configurations, *Water Resour. Res.*, 43, W10437, doi:10.1029/2007WR005907.
- Bolla Pittaluga, M., R. Repetto, and M. Tubino (2003), Channel bifurcations in braided rivers: Equilibrium configurations and stability, *Water Resour. Res.*, 39(3), 1046, doi:10.1029/2001WR001112.
- Bridge, J. S. (1993), The interaction between channel geometry, water flow, sediment transport and deposition in braided rivers, in *Braided Rivers*, edited by J. L. Best and C. S. Bristow, pp. 14–73, Geol. Soc. of Am., Boulder, Colo.
- Dade, W. B., and P. F. Friend (1998), Grain-size, sediment-transport regime, and channel slope in alluvial rivers, *J. Geol.*, 106, 661–675.

- Dargahi, B. (2004), Three-dimensional flow modelling and sediment transport in the River Klaralven, *Earth Surf. Processes Landforms*, 29, 821–852.
- Davoren, A., and M. P. Mosley (1986), Observations of bedload movement, bar development and sediment supply in the braided Ohau River, *Earth Surf. Processes Landforms*, 11, 643–652.
- Edmonds, D. A., R. Slingerland, and R. M. Desibour (2004), Geometric properties of bifurcating delta distributary channels, *Eos Trans. AGU*, 85, Fall Meet. Suppl., H43A-0367.
- Edmonds, D. A., and R. L. Slingerland (2007), Mechanics of river mouth bar formation: Implications for the morphodynamics of delta distributary networks, *J. Geophys. Res.*, 112, F02034, doi:10.1029/2006JF000574.
- Ericson, J. P., C. J. Vorosmarty, S. L. Dingman, L. G. Ward, and M. Meybeck (2006), Effective sea-level rise and deltas: Causes of change and human dimension implications, *Global Planet. Change*, 50, 63–82.
- Federici, B., and C. Paola (2003), Dynamics of channel bifurcations in noncohesive sediments, *Water Resour. Res.*, 39(6), 1162, doi:10.1029/2002WR001434.
- Frings, R., and M.G. Kleinhans (2008), Complex variations in sediment transport at three large river bifurcations during discharge waves in the river Rhine, *Sedimentology*, 1–27, doi:10.1111/j.1365-3091.2007.00940.x
- Hall, P. (2005), On the non-parallel instability of sediment-carrying channels of slowly varying width, *J. Fluid Mech.*, 529, 1–32.
- Hardy, R., S. Lane, S. Ferguson, and D. Parsons (2003), Assessing the credibility of a series of computational fluid dynamic simulations of open channel flow, *Hydrol. Processes*, 17, 1539–1560.
- Hibma, A., H. M. Schuttelaars, and H. J. De Vriend (2004), Initial formation and long-term evolution of channel-shoal patterns, *Cont. Shelf Res.*, 24, 1637–1650.
- Ikeda, S. (1982), Incipient motion of sand particles on side slopes, *J. Hydraul. Div.*, 108, 95–114.
- Information Service Corporation of Saskatchewan (2003), Aerial photographs of Mossy Delta in Lake Cumberland, Geomatics Distribution Centre, Regina, Sask., Canada.
- Islam, G. M. T., M. R. Kabir, and A. Nishat (2006), Nodal point relation for the distribution of sediments at channel bifurcation, *J. Hydraul. Eng.*, 132, 1105.
- Kleinhans, M. G., B. Jagers, E. Mosselman, and K. Sloff (2008), Bifurcation dynamics and avulsion duration in meandering rivers by 1D and 3D models, *Water Resour. Res.*, doi:10.1029/2007WR005912, in press.
- Krone, R. B. (1962), Flume studies of the transport of sediment in estuarial shoaling processes, Final Report, pp. 1–41, Hydraulic Engineering Laboratory and Sanitary Engineering Research Laboratory, University of California, Berkeley.
- Lesack, L. F. W., and P. Marsh (2007), Lengthening plus shortening of river-to-lake connection times in the Mackenzie River Delta respectively via two global change mechanisms along the arctic coast, *Geophys. Res. Lett.*, 34, L23404, doi:10.1029/2007GL031656.
- Lesser, G., J. Roelvink, J. Van Kester, and G. Stelling (2004), Development and validation of a three-dimensional morphological mode, *Coastal Eng.*, 51, 883–915.
- Marciano, R., Z. B. Wang, A. Hibma, H. J. De Vriend, and A. Defina (2005), Modeling of channel patterns in short tidal basins, *J. Geophys. Res.*, 110, F01001, doi:10.1029/2003JF000092.
- Miori, S., R. Repetto, and M. Tubino (2006), A one-dimensional model of bifurcations in gravel bed channels with erodible banks, *Water Resour. Res.*, 42, W11413, doi:10.1029/2006WR004863.
- Miori, S., W. Bertoldi, R. Repetto, L. Zanoni, and M. Tubino (2007), The effect of alternating bars migration on river bifurcation dynamics, *Eos Trans. AGU*, 88.
- Mosselman, E., M. Huisink, E. Koomen, and A. C. Seijmonsbergen (1995), Morphological changes in a large braided sand-bed river, in *River Geomorphology*, edited by E. J. Hickin, pp. 235–249, Wiley, Chichester, UK.
- Olson, D. M., and E. Dinerstein (1998), The Global 200: A representation approach to conserving the earth's most biologically valuable ecoregions, *Conserv. Biol.*, 12, 502–515.
- Oosterlaan, S., and M. Meyers (1995), Evolution of the Mossy delta in relation to hydrodam construction and lake level fluctuation, Senior thesis, 29 pp, University of Illinois-Chicago, Chicago, Ill.
- Parker, G. (1978), Self-formed straight rivers with equilibrium banks and mobile bed: part 2. The gravel river, *J. Fluid Mech.*, 89, 127–146.
- Partheniades, E. (1965), Erosion and deposition of cohesive soils, *J. Hydraul. Div., ASCE*, 91, 105–139.
- Repetto, R., M. Tubino, and C. Paola (2002), Planimetric instability of channels with variable width, *J. Fluid Mech.*, 457, 79–109.
- Richardson, W. R., and C. R. Thorne (2001), Multiple thread flow and channel bifurcation in a braided river: Brahmaputra-Jamuna River, Bangladesh, *Geomorphology*, 38, 185–196.
- Slingerland, R., and N. D. Smith (1998), Necessary conditions for a meandering-river avulsion, *Geology*, 26, 435–438.
- Sloff, C. J., M. Bernabe, and T. Baur (2003), On the stability of the Panmerdense Kop river bifurcation, *Proc. 3rd IAHR Symposium on River, Coastal and Estuarine Morphodynamics: Proceedings RCEM 2003*, Barcelona, Spain.
- Syvitski, J., C. J. Vorosmarty, A. J. Kettner, and P. Green (2005), Impact of humans on the flux of terrestrial sediment to the global coastal ocean, *Science*, 308, 376–380.
- Van Maren, D. S. (2005), Barrier formation on an actively prograding delta system: The Red River Delta, Vietnam, *Mar. Geol.*, 224, 123–143.
- van Rijn, L. C. (1984), Sediment transport: part I. Bed load transport, *J. Hydraul. Eng.*, 110, 1431–1456.
- Wang, Z. B., R. J. Fokkink, M. Devries, and A. Langerak (1995), Stability of river bifurcations in 1D morphodynamic models, *J. Hydraul. Res.*, 33, 739–750.
- Wu, F., and T. Yeh (2005), Forced bars induced by variations of channel width: Implications for incipient bifurcation, *J. Geophys. Res.*, 110, F02009, doi:10.1029/2004JF000160.
- Zanichelli, G., E. Caroni, and V. Fiorotto (2004), River bifurcation analysis by physical and numerical modeling, *J. Hydraul. Eng.-ASCE*, 130, 237–242.
- Zolezzi, G., W. Bertoldi, and M. Tubino (2006), Morphological analysis and prediction of river bifurcations, in *Braided Rivers: Process, Deposits, Ecology and Management*, edited by C. Bristow et al., pp. 233–256, Blackwell Publishing, Oxford, England.

---

D. A. Edmonds and R. L. Slingerland, Department of Geosciences, Pennsylvania State University, 513 Deike Building, University Park, PA 16802, USA. (dedmonds@geosc.psu.edu)